2026 IEEE International Conference on Robotics and Automation (ICRA 2026)
June 1-5, 2026. Vienna, Austria

Safe Robotics Control with Directional Projection Control Barrier Functions via Differentiable Optimization

Yan Wei , Jiajie Yao , Xinyi Yu , Linlin Ou

Abstract— **Collision avoidance is essential for robotic systems. This paper presents a method for designing directional projection control barrier functions (CBFs) based on differentiable optimization for second-order robotic systems. The approach reduces high-order CBFs to first-order ones and estimates collision risk by examining the intersection of projections along the relative velocity direction. Under the assumption that both the target and obstacles are convex polyhedra whose projections yield convex polygons, a tunable uniform scaling function, centered at the centroid, is introduced to pad the convex polygon. The strict convexity of this padded region is rigorously proven. Using the minimum scaling factor that leads to intersection between two projected convex polygons, a CBF is constructed and incorporated into a tracking controller to ensure collision avoidance. The effectiveness of the proposed method is validated through simulations with a 2D mobile robot and a 7-DOF Franka manipulator.**

I. INTRODUCTION

With the rapid advancement of robotic technology, the application scenarios of intelligent robots in industrial [1], medical, and service fields have expanded, making safety a critical challenge [2], particularly in areas such as collision avoidance in dynamic environments and human-robot interaction safety. To ensure reliable operation of robots in complex environments, various safety control methods have been proposed, such as model predictive control (MPC) [3], reachability analysis [4], and artificial potential fields [5]. However, the computational burden and limited prediction horizon of MPC restrict its real-time applicability, the high-dimensional computational complexity of reachability analysis limits its practical use, and artificial potential fields are prone to local minima issues. In contrast, control barrier functions (CBFs) offer a lightweight solution with theoretical safety guarantees [6]. By constructing forward-invariant safe sets, CBFs can be efficiently integrated with other control objectives and have been widely adopted in safety-critical applications.

Regarding obstacle avoidance methods, existing CBFs typically rely on Euclidean shortest distances, which are only applicable to simple convex primitives such as points, spheres, or capsules. This often results in overly conservative safe sets and lacks a clear definition when objects overlap. In practical applications, complex objects must be approximated as combinations of multiple simple convex primitives, which introduces computational redundancy and conservatism. In [7], a differentiable collision detection framework was proposed for two convex primitives, which solves the minimum scaling factor by convex optimization. However, because of the presence of planar and vertex features in convex primitives, the continuity and differentiability of the solution remain questionable. Previous works [8], [9] demonstrated that the minimum scaling factor of a strongly convex scaling function exhibits continuous differentiability and proposed a CBF defined using this scaling factor, successfully applying it to obstacle avoidance tasks. For more general safety constraints involving arbitrary relative degrees, higher-order CBFs (HOCBFs) have been introduced [10] and their robustness has also been investigated [11]. Nevertheless, the prevailing method of HOCBFs introduces complexity and potential feasibility issues [12].

Existing CBF designs often focus on local safety optimization at the current moment, exhibiting myopia that may sacrifice global performance, such as path optimality. For dynamic and uncertain environments, a common strategy is the collision cone method[13]. This approach evaluates collision risk by examining the geometric relationship between the relative velocity vector and a cone-shaped collision region, enabling dynamic trajectory adjustment to prevent collisions. Meanwhile, considering the limitations of steering or thrust capabilities in system dynamics, effectively avoiding moving obstacles remains challenging. Previous studies [14], [15] have developed and empirically validated collision cone CBFs (C3BFs) to facilitate real-time kinematic obstacle avoidance for nonholonomic ground vehicles. Further extending this concept, the work [16] applied C3BFs to 3D scenarios, specifically for unmanned aerial vehicles. Nevertheless, these methods often yield overly conservative safety sets, primarily because they simplify the ego vehicle as a point mass and approximate obstacles with circles or spheres. Inspired by the strengths of differentiable optimization and the collision cone framework, this work seeks to overcome these limitations.

Inspired by the above studies, this paper focuses on a CBFs design method for safety control of second-order robotic systems, particularly obstacle avoidance between polyhedra in dynamic environments. The main contributions of this paper are summarized as follows.

- For second-order robotic systems, a directional projection CBFs design method based on differentiable

This research was supported by the National Natural Science Foundation of China under Grants 62373329, 62203392, the Zhejiang Natural Science Foundation under Grant LZ25F030003, and the Baima Lake Laboratory Joint Funds of the Zhejiang Provincial Natural Science Foundation under Grant No. LBMHD24F030002.(Corresponding author: Linlin Ou)

Y. Wei, J. Yao, X. Yu, and L. Ou are with the College of Information Engineering, Zhejiang University of Technology, Hangzhou310023, China (e-mail: weiyanok@zjut.edu.cn; 2111240301l2@zjut.edu.cn; yuxy@zjut.edu.cn; linlinou@zjut.edu.cn).

optimization is proposed. The approach explicitly incorporates the geometry of both the robot and obstacles, enabling collision avoidance in dynamic environments.
- A tunable uniform scaling function with scaling about a centroid is designed for padding convex polygons, with its strict convexity rigorously proven.
- The collision risk is assessed by the extent of projection intersection along the relative velocity direction, effectively addressing the short-sightedness of traditional Euclidean distance metrics.

Notations: $\|\cdot\|$ is the ℓ_2 norm of a vector or a matrix, and $(\cdot)^\dagger$ is the pseudoinverse of a matrix. $\mathbb{N}_{>0}$ is the set of positive integers. $\mathbf{I}$ is the identity matrix with proper dimensions. An extended $\mathcal{K}_\infty$ function Γ is a continuous strictly increasing function that maps $\mathbb{R}$ to $\mathbb{R}$ with $\Gamma(0)=0$. $\mathcal{C}^1$ denotes continuously differentiable and $\mathcal{C}^2$ denotes twice continuously differentiable. For a $\mathcal{C}^1$ function $h\colon \mathbb{R}^n \to \mathbb{R}$, its gradient ∇h is a column vector while the partial derivative $\frac{\partial h}{\partial x}$ is a row vector. For a $\mathcal{C}^1$ function $f\colon \mathbb{R}^n \to \mathbb{R}^m$, the partial derivative $\frac{\partial f}{\partial x}$ is an $m \times n$ matrix.

II. Preliminaries

A. Control Barrier Function

Consider a control-affine system

$$\dot{x} = f(x) + g(x)u, \tag{1}$$

with $f : \mathbb{R}^n \to \mathbb{R}^n$ and $g : \mathbb{R}^n \to \mathbb{R}^{n\times m}$ being locally Lipschitz, the states $x \in \mathcal{X} \subset \mathbb{R}^n$, and the control $u \in \mathcal{U} \subset \mathbb{R}^m$.

Let $h : \mathcal{X} \subset \mathbb{R}^n \to \mathbb{R}$ be a $\mathcal{C}^1$ function, and define

$$C = \{x \in \mathcal{X} \mid h(x) \geq 0\}, \tag{2a}$$
$$\partial C = \{x \in \mathcal{X} \mid h(x) = 0\}, \tag{2b}$$
$$\text{Int}(C) = \{x \in \mathcal{X} \mid h(x) > 0\}, \tag{2c}$$

where C is the *safe set*, ∂C is the boundary of C, and $\text{Int}(C)$ is the interior of C. It is assumed that $\text{Int}(C) \neq \varnothing$ and $\nabla h(x) \neq 0$ for $x \in \partial C$. Then, the safety of system (1) is guaranteed and the set C is called safe set.

Definition 1 (Relative Degree [17]): For a $\mathcal{C}^1$ function $h : \mathcal{X} \to \mathbb{R}$ with respect to system (1), the relative degree is defined as the minimum number of times $h(x)$ needs to be differentiated along the system dynamics until the control input u explicitly appears in the resulting derivative.

When the relative degree of function $h(x)$ is $r \in \mathbb{N}_{>0}$, and the inequality $h(x) \geq 0$ is used as a safety constraint, the definition of CBF for $r = 1$ is given as follows.

Definition 2 (Control Barrier Function [6]): A $\mathcal{C}^1$ function $h : \mathcal{X} \to \mathbb{R}$ constitutes a CBF if there exists an extended class $\mathcal{K}_\infty$ function Γ such that for system (1)

$$\sup_{u\in\mathcal{U}} [L_f h(x) + L_g h(x) u] \geq -\Gamma(h(x)), \quad \forall x \in C \tag{3}$$

where $L_f h(\cdot) = \frac{\partial h}{\partial x} f(\cdot)$ denotes the Lie derivative of h with respect to f. For simplicity, the right-hand side of (3) can be reduced to $-\gamma h(x)$ with $\gamma > 0$.

Given a CBF h, the set of admissible controls is defined as:

$$K_{cbf}(x) = \{u \in \mathcal{U} \mid L_f h(x) + L_g h(x) u \geq -\Gamma(h(x))\}. \tag{4}$$

The control $u \in K_{cbf}(x)$ renders C forward-invariant provided the initial condition $x_0 \in C$.

B. Problem Statement

Consider an second-order nonlinear system

$$\begin{cases} \dot{x}_1 = x_2 \\ \dot{x}_2 = f_2(x) + g_2(x)u \end{cases}, \tag{5}$$

with $f_2 : \mathbb{R}^{2n} \to \mathbb{R}^n$ and $g_2 : \mathbb{R}^{2n} \to \mathbb{R}^{n\times m}$ being locally Lipschitz, the states $x = (x_1, x_2)^\top \in \mathcal{X} \subset \mathbb{R}^{2n}$, and the control $u \in \mathcal{U} \subset \mathbb{R}^n$.

For systems (5), the primary motivation for adopting HOCBF arises the first derivative of a standard CBF does not explicitly include control input terms, thus requiring higher-order differentiation. Now, first-order state derivatives (e.g., velocity) are directly incorporated as independent variables in the CBF formulation.

This paper aims to avoid collisions between polyhedral objects in dynamic environments and to take evasive actions in advance within a certain time period before a collision occurs. The objective is to find a CBF $h : \mathcal{X} \to \mathbb{R}$, there exists an extended class $\mathcal{K}_\infty$ function Γ such that

$$\begin{aligned} \sup_{u\in\mathcal{U}} \frac{\partial h}{\partial x_2} f_2(x) + \frac{\partial h}{\partial x_2} g_2(x) u + \frac{\partial h}{\partial x_1} x_2 \\ \geq -\Gamma(h(x)), \quad \forall x \in C. \end{aligned} \tag{6}$$

The set of admissible controls is given by

$$K_{cbf}(x) = \left\{ u \in \mathcal{U} \;\middle|\; \begin{aligned} \sup_{u\in\mathcal{U}} \Big[\frac{\partial h}{\partial x_2} f_2(x) + \frac{\partial h}{\partial x_2} g_2(x) u \\ + \frac{\partial h}{\partial x_1} x_2 \Big] \geq -\Gamma(h(x)) \end{aligned} \right\}. \tag{7}$$

The control $u \in K_{cbf}(x)$ renders C forward-invariant provided the initial condition $x_0 \in C$. Evidently, compared to HOCBF, this CBF requires designing only one class $\mathcal{K}_\infty$ function.

III. DIFFERENTIABLE OPTIMIZATION

This section introduces differentiable optimization, with the scaling function redefined to establish its physical significance.

Definition 3 (Scaling functions): A class $\mathcal{C}^2$ function $\mathcal{F}_A : \mathbb{R}^n \to \mathbb{R}$ is termed a scaling function for a non-empty closed set $A \subset \mathbb{R}^n$ if

1) $A = \{z \in \mathbb{R}^n \mid \mathcal{F}_A(z) \leq \alpha, \alpha \in \mathbb{R}^+\}$;
2) $\exists! z_0 \in \mathbb{R}^n$ such that $\forall \alpha > 0, \mathcal{F}_A(z_0) = 0$;
3) $\mathcal{F}_A(z) \geq 0$ for all $z \in \mathbb{R}^n$.

This definition establishes a concrete connection between the abstract mathematical functions and the intuitive physical concept of uniform scaling. The point z_0 is designated as the *scaling center* of set A, where $\alpha = 1$ corresponds to the *original size* of A, $\alpha > 1$ represents a *uniform scaling up* of A centered at z_0, and $\alpha < 1$ represents a *uniform scaling down* of A centered at z_0.

Certain sets possess a natural representation for scaling functions. For a 2D (or 3D) ball of radius r, the scaling function is given by $\mathcal{F}_A(z) = (z - z_0)^\top P(z - z_0)$, where the scaling center z_0 corresponds to the ball's centroid and $P = I/r^2$. Similarly, the scaling function for an ellipse (or ellipsoid) can be derived by appropriate selection of the matrix P. The following revised lemma is introduced:

Lemma 1 ([9]): Given a convex scaling function $\mathcal{F}_A$, for any z such that $\mathcal{F}_A(z) > \alpha$ ($\alpha > 0$), $\frac{\partial \mathcal{F}_A}{\partial z}(z) \neq 0$.

Let $\mathcal{F}_A$ and $\mathcal{F}_B$ be two convex scaling functions associated with A and B. Assume that the scaling centers of sets A and B are distinct, i.e., $c_A \neq c_B$, where c_A and c_B denote the scaling centers of A and B. The minimum uniform scaling factor that causes the boundaries of sets A and B to intersect can be obtained by solving the following optimization problem [8].

$$\begin{aligned} &\min_{z,\alpha} \ \alpha \\ &\text{s.t.} \quad \mathcal{F}_A(z) \leq \alpha, \\ &\qquad \mathcal{F}_B(z) \leq \alpha. \end{aligned} \tag{8}$$

Let α^* be the solution to the problem in (8). Fig. 1 presents two cases of the solution: (a) when $\alpha^* > 1$, indicating that the sets need to be scaled up to intersect; (b) when $\alpha^* < 1$, indicating that the sets can be scaled down while still intersecting. The Lagrangian function of the above problem

(a) $\alpha^* > 1$ (b) $\alpha^* < 1$

Fig. 1: The minimum scaling optimization problem for two circular sets A and B. The original sets are depicted in darker colors, while the scaled sets are shown in lighter colors, with their intersection highlighted in red. (a) illustrates boundary intersection after scaling up, while (b) demonstrates boundary intersection after scaling down.

(8) is given as follows:

$$L(\alpha, z, \lambda_A, \lambda_B) = \alpha + \lambda_A \left(\mathcal{F}_A(z) - \alpha\right) + \lambda_B \left(\mathcal{F}_B(z) - \alpha\right), \tag{9}$$

where λ_A and λ_B are the Lagrange multipliers associated with the constraints $\mathcal{F}_A(z) \geq \alpha$ and $\mathcal{F}_B(z) \geq \alpha$, respectively.

Since the problem is convex and strictly feasible (i.e., Slater's condition holds), the Karush-Kuhn-Tucker (KKT) conditions are necessary. The optimal primal (α^*, z^*) and dual $(\lambda_A^*, \lambda_B^*)$ variables satisfy the following KKT conditions:

$$\lambda_A^* + \lambda_B^* = 1, \tag{10a}$$
$$\lambda_A^* \frac{\partial \mathcal{F}_A}{\partial z}(z^*) + \lambda_B^* \frac{\partial \mathcal{F}_B}{\partial z}(z^*) = 0, \tag{10b}$$
$$\lambda_A^* (\mathcal{F}_A(z^*) - \alpha^*) = 0, \tag{10c}$$
$$\lambda_B^* (\mathcal{F}_B(z^*) - \alpha^*) = 0, \tag{10d}$$
$$\lambda_A^*, \lambda_B^* \geq 0. \tag{10e}$$

The following revised lemma is introduced:

Lemma 2 ([9]): If $\mathcal{F}_A$ and $\mathcal{F}_B$ are both convex and $c_A \neq c_B$, then $\lambda_A^*, \lambda_B^* > 0$, $\mathcal{F}_A(z^*) = \mathcal{F}_B(z^*) = \alpha^*$, and $\frac{\partial \mathcal{F}_A}{\partial z}(z^*) \neq \frac{\partial \mathcal{F}_B}{\partial z}(z^*)$.

Assume that the scaling functions $\mathcal{F}_A$ and $\mathcal{F}_B$ are also functions of a parameter vector θ. The following theorem establishes the continuous differentiability of α^* with respect to θ.

Theorem 1 ([9]): Assume that $c_A \neq c_B$, and $\mathcal{F}_A$ and $\mathcal{F}_B$ are also $\mathcal{C}^2$ in θ. If $\mathcal{F}_A$ and $\mathcal{F}_B$ are both convex w.r.t. z and one of them is strictly convex w.r.t. z, then α^* is continuously differentiable w.r.t. θ

$$\frac{\partial \alpha^*}{\partial \theta}(\theta) = \frac{\partial \mathcal{F}_A}{\partial z}(z^*, \theta) \frac{\partial z^*}{\partial \theta}(\theta) + \frac{\partial \mathcal{F}_A}{\partial \theta}(z^*, \theta). \tag{11}$$

$\frac{\partial z^*}{\partial \theta}$ is given by the following equation

$$\underbrace{\begin{bmatrix} M & c \\ c^\top & 0 \end{bmatrix}}_{N} \begin{bmatrix} \frac{\partial z^*}{\partial \theta} \\ \frac{\partial \lambda_A^*}{\partial \theta} \end{bmatrix} = \begin{bmatrix} \Omega_1 \\ \Omega_2 \end{bmatrix}, \tag{12}$$

where

$$M = \lambda_A^* \frac{\partial^2 \mathcal{F}_A}{\partial z^2}(z^*, \theta) + (1 - \lambda_A^*) \frac{\partial^2 \mathcal{F}_B}{\partial z^2}(z^*, \theta), \tag{13a}$$
$$c = \frac{\partial \mathcal{F}_A}{\partial z}(z^*, \theta)^\top - \frac{\partial \mathcal{F}_B}{\partial z}(z^*, \theta)^\top, \tag{13b}$$
$$\Omega_1 = -\lambda_A^* \frac{\partial^2 \mathcal{F}_A}{\partial z \partial \theta}(z^*, \theta) - (1 - \lambda_A^*) \frac{\partial^2 \mathcal{F}_B}{\partial z \partial \theta}(z^*, \theta), \tag{13c}$$
$$\Omega_2 = -\frac{\partial \mathcal{F}_A}{\partial \theta}(z^*, \theta) + \frac{\partial \mathcal{F}_B}{\partial \theta}(z^*, \theta). \tag{13d}$$

IV. SCALING FUNCTIONS FOR 2D CONVEX POLYGONS

This section derives a scaling function for 2D convex polygons. The main idea involves padding the polygon into a strictly convex set with tunable accuracy, while enabling uniform scaling.

A. Candidate Scale Functions

In the 2D plane, a convex polygon S with N edges can be delimited by N linear inequalities corresponding to each of its edges, i.e., $S = \{z \in \mathbb{R}^2 \mid Fz \leq b\}$ where $F \in \mathbb{R}^{N \times 2}$ and $b \in \mathbb{R}^N$. Given the vertex coordinates $\theta = [x_1, y_1, ..., x_N, y_N] \in \mathbb{R}^{2N}$ of S in a counterclockwise order, $F(\theta)$ and $b(\theta)$ can be given by the following expressions [9]:

$$\underbrace{\begin{bmatrix} y_2 - y_1 & x_1 - x_2 \\ y_3 - y_2 & x_2 - x_3 \\ \vdots & \vdots \\ y_1 - y_N & x_N - x_1 \end{bmatrix}}_{F(\theta)} \begin{bmatrix} x \\ y \end{bmatrix} \leq \underbrace{\begin{bmatrix} x_1 y_2 - x_2 y_1 \\ x_2 y_3 - x_3 y_2 \\ \vdots \\ x_N y_1 - x_1 y_N \end{bmatrix}}_{b(\theta)}, \tag{14}$$

where $F(\theta) \in \mathbb{R}^{N\times 2}$ and $b(\theta) \in \mathbb{R}^N$, $\frac{\partial F}{\partial \theta}$ and $\frac{\partial b}{\partial \theta}$ exist and are continuous in θ. Let the i-th row of F and b be F_i and b_i, respectively.

Next, a scaling function $\mathcal{F}(z)$ is derived to determine whether a point z lies inside a polygon uniformly scaled by factor α.

A polygon is uniformly scaled by α, subject to the following constraints [7]:

$$FQ^T(z-c) \leq \alpha b, \tag{15}$$

where the rotation matrix $Q \in \mathbb{R}^{2\times 2}$ transforms between the world coordinate system and the coordinate system centered at the polygon's centroid c.

The centroid of a polygon $c = (x_c, y_c)$ can be calculated using the following formulas:

$$x_c = \frac{1}{6A}\sum_{i=1}^{N}(x_i + x_{i+1})(x_i y_{i+1} - x_{i+1}y_i), \tag{16a}$$

$$y_c = \frac{1}{6A}\sum_{i=1}^{N}(y_i + y_{i+1})(x_i y_{i+1} - x_{i+1}y_i), \tag{16b}$$

where the signed area A of the polygon is calculated as $A = \frac{1}{2}\sum_{i=1}^{N}(x_i y_{i+1} - x_{i+1}y_i)$. If the vertices are ordered clockwise, A will be negative. If ordered counterclockwise, A will be positive. Typically, the absolute value $|A|$ is used for centroid calculations.

Lemma 3: Assume that the vertices θ of the convex polygon S are arranged counterclockwise. If the origin of the coordinate system in which the vertices are defined lies inside the polygon, then $b > 0$ in the inequality (14).

Proof: When the coordinate system is translated such that its origin coincides with the interior point $c = (x_c, y_c)$, the vertex coordinates become $\tilde{x}_i = x_i - x_c$ and $\tilde{y}_i = y_i - y_c$ for $i = 1, \ldots, N$. The new coefficients $\tilde{b}_i$ are defined as:

$$\tilde{b}_i = \tilde{x}_i\tilde{y}_{i+1} - \tilde{x}_{i+1}\tilde{y}_i. \tag{17}$$

Geometrically, $\tilde{b}_i$ represents twice the signed area of the triangle formed by points c, v_i, and v_{i+1}. The signed area A_i of triangle (c, v_i, v_{i+1}) can be computed using the determinant formula:

$$A_i = \frac{1}{2}\begin{vmatrix} 1 & 0 & 0 \\ 1 & \tilde{x}_i & \tilde{y}_i \\ 1 & \tilde{x}_{i+1} & \tilde{y}_{i+1} \end{vmatrix} = \frac{1}{2}(\tilde{x}_i\tilde{y}_{i+1} - \tilde{x}_{i+1}\tilde{y}_i), \tag{18}$$

which confirms that $\tilde{b}_i = 2A_i$.

Since the polygon is convex with vertices ordered counterclockwise and c is an interior point, every triangle (c, v_i, v_{i+1}) is positively oriented. Therefore, each signed area $A_i > 0$, implying $\tilde{b}_i > 0$ for all $i = 1, \ldots, N$. ∎

Naturally, a candidate scale function is defined as

$$f(z) = \max_{i=1,\ldots,N}\left(\frac{F_i(z-c)}{b_i}\right), \tag{19}$$

where the point c represents the centroid of the polygon, which also serves as the scaling center. F_i and b_i are expressed in a coordinate system centered at the centroid. Since the centroid lies strictly inside the polygon, by Lemma 3 $b_i > 0$. However, the function (19) is non-differentiable, which will be addressed in the next subsection.

B. Padding the Polygon Into a Strictly Convex Set

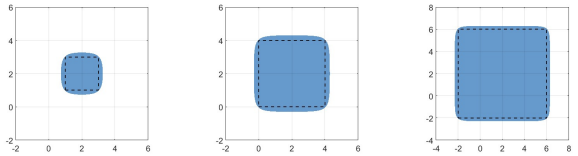

(a) $\alpha = 0.65$, $\kappa = 5$ (b) $\alpha = 1.15$, $\kappa = 5$ (c) $\alpha = 2.15$, $\kappa = 5$

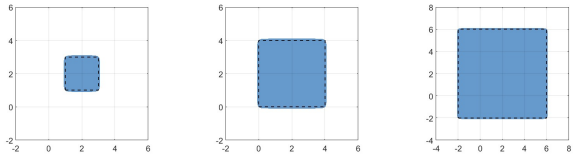

(d) $\alpha = 0.55$, $\kappa = 15$ (e) $\alpha = 1.05$, $\kappa = 15$ (f) $\alpha = 2.05$, $\kappa = 15$

Fig. 2: Padded squares with different α and κ. (a), (d) show padded-shrunk shapes; (b), (e) show original padded shapes; (c), (f) show padded-expanded shapes.

The next step is to convert the 2D convex polygon

$$S = \{z \in \mathbb{R}^2 \mid \max_{i=1,\ldots,N}\left(\frac{F_i(z-c)}{b_i}\right) \leq \alpha\} \tag{20}$$

with $\alpha > 0$, into a strictly convex set. Consider using LogSumExp to approximate max, resulting in a set

$$S_s = \left\{z \in \mathbb{R}^2 \;\middle|\; \frac{1}{\kappa}\ln\left(\sum_{i=1}^{N} e^{\kappa\cdot\frac{F_i(z-c)}{b_i}}\right) \leq \alpha\right\} \tag{21}$$

with $\kappa > 0$, $\alpha > 0$. Since Logsumexp [18] is a smooth upper bound of max, it follows that $S_s \subset S$, which is not the desired result. In fact, by adding a small positive offset δ (determined by κ) to α, the new set ${S_s}^*$ satisfies ${S_s}^* \supset S$ where

$${S_s}^* = \left\{z \in \mathbb{R}^2 \;\middle|\; \frac{1}{\kappa}\ln\left(\sum_{i=1}^{N} e^{\kappa\cdot\frac{F_i(z-c)}{b_i}}\right) \leq \alpha + \delta\right\} \tag{22}$$

with $\kappa > 0$, $\alpha > 0$, $\delta > 0$.

The scaling function for S_s is defined as

$$\mathcal{F}_{S_s}(z) = \frac{1}{\kappa}\ln\left(\sum_{i=1}^{N} e^{\kappa\cdot\frac{F_i(z-c)}{b_i}}\right), \tag{23}$$

where $S_s = \left\{z \in \mathbb{R}^2 \mid \mathcal{F}_{S_s}(z) \leq \alpha, \alpha > 0\right\}$ follows directly from the definition of S_s.

Theorem 2: Assume that the vertices θ of the convex polygon S are arranged counterclockwise. If the origin of the coordinate system in which the vertices are defined lies inside the polygon, then $\frac{\partial^2 \mathcal{F}_{S_s}}{\partial z^2}(z) > 0$, i.e., $\mathcal{F}_{S_s}$ is strictly convex w.r.t. z.

Proof: Strict convexity of $\mathcal{F}_{S_s}(z)$ is proven by showing that its Hessian matrix is positive definite. Let $U = \sum_{i=1}^{N} e^{\kappa \cdot \frac{F_i(z-c)}{b_i}}$, $\dot{U} = \kappa \sum_{i=1}^{N} \frac{F_i}{b_i} \exp\left(\kappa \cdot \frac{F_i(z-c)}{b_i}\right)$, $\ddot{U} = \kappa^2 \sum_{i=1}^{N} \frac{F_i^\top \cdot F_i}{b_i^2} \exp\left(\kappa \cdot \frac{F_i(z-c)}{b_i}\right)$, the second partial derivative of $\mathcal{F}_{S_s}$ with respect to z is given as follows:

$$\frac{\partial^2 \mathcal{F}_{S_s}}{\partial z^2}(z) = \frac{U \cdot \ddot{U} - \dot{U}^\top \cdot \dot{U}}{\kappa \ \cdot U^2}. \tag{24}$$

Since $\kappa \ \cdot U^2 > 0$, the Hessian matrix is defined as

$$\mathbf{H} = U \cdot \ddot{U} - \dot{U}^\top \cdot \dot{U}. \tag{25}$$

For any non-zero vector $d \in \mathbb{R}^2$, we have:

$$d^\top \mathbf{H}\, d = d^\top \left[U \cdot \ddot{U} - \dot{U}^\top \dot{U}\right] d. \tag{26}$$

Let $w_i = \exp\left(\kappa \frac{F_i(z-c)}{b_i}\right) > 0$ and $a_i = \frac{F_i d}{b_i}$. Then,

$$d^\top \ddot{U}\, d = \kappa^2 \sum_{i=1}^{N} \frac{(F_i d)^2}{b_i^2} w_i = \kappa^2 \sum_{i=1}^{N} a_i^2 w_i, \tag{27}$$

$$d^\top (\dot{U})^\top \dot{U}\, d = (\dot{U} d)^2 = \kappa^2 \left(\sum_{i=1}^{N} a_i w_i\right)^2. \tag{28}$$

Thus, (26) can be changed as:

$$d^\top \mathbf{H}\, d = \kappa^2 \left[\left(\sum_{k=1}^{N} w_k\right)\left(\sum_{i=1}^{N} a_i^2 w_i\right) - \left(\sum_{j=1}^{N} a_j w_j\right)^2\right]. \tag{29}$$

By the Cauchy-Schwarz inequality [19], it follows that

$$\left(\sum_{j=1}^{N} a_j w_j\right)^2 \leq \left(\sum_{k=1}^{N} w_k\right)\left(\sum_{i=1}^{N} a_i^2 w_i\right), \tag{30}$$

where inequality holds iff all a_i are equal. For a strictly convex polygon, the edges cannot be all parallel, $\exists i, j$ such that $\frac{F_i}{b_i} \neq \lambda \frac{F_j}{b_j}$ for any λ. Thus, $\forall d \neq 0$, $a_i = \frac{F_i d}{b_i}$ cannot be constant across all i. Consequently,

$$\left(\sum_{k=1}^{N} w_k\right)\left(\sum_{i=1}^{N} a_i^2 w_i\right) - \left(\sum_{j=1}^{N} a_j w_j\right)^2 > 0. \tag{31}$$

Hence, $\mathbf{H}$ is positive definite, and $\mathcal{F}_{S_s}(z)$ is strictly convex. ■

As shown in Fig. 2, the precision of the padded shape ${S_s}^*$ can be adjusted through the parameter κ, where increasing κ results in higher precision while requiring a smaller offset δ. This method can also be applied to 3D convex polytopes using the inequalities describing each face of the polytope.

When $\mathcal{F}_A = \kappa \cdot \exp\left(\mathcal{F}_{S_s}\right)$ and $\mathcal{F}_B = \kappa \cdot \exp\left(\mathcal{F}_{S_s'}\right)$, optimization problem (8) is equivalent to

$$\begin{aligned} &\min_{z,\alpha'} \ \kappa \cdot \exp(\alpha) \\ &\text{s.t.}\ \mathcal{F}_{S_s}(z) \leq \kappa \cdot \exp(\alpha), \quad \mathcal{F}_{S_s'}(z) \leq \kappa \cdot \exp(\alpha), \end{aligned} \tag{32}$$

with $\alpha' = \kappa \cdot \exp(\alpha)$ as $\alpha > 1$ if $S_s \cap S_s' = \varnothing$. The constraint $\mathcal{F}_{S_s}(z) \leq \alpha$ (same for $\mathcal{F}_{S_s'}(z) \leq \alpha$) can be further developed into a sum of exponential cones and this can be efficiently solved by solvers such as splitting conic solver and embedded conic solver.

V. Directional Projection Control Barrier Functions

In this section, a innovative directional projection CBFs construction method is proposed.

Consider two convex polyhedral objects denoted as A and B, here represented as cuboids for illustration, where A is the controlled object and B is an obstacle. Consider the system (1), denote $x = [x_1, x_2]^T$, where x_1 and x_2 denote position $\mathbf{x}$ and velocity $\mathbf{v}$.

Each object defines an additional body-fixed reference frame with its origin $\mathbf{r}_A \in \mathbb{R}^3$ and $\mathbf{r}_B \in \mathbb{R}^3$ located at their respective centroids, referenced to the world coordinate frame W. The orientation of each object is defined by rotation matrices ${}^W\mathbf{R}_A \in \mathbb{R}^{3\times3}$ and ${}^W\mathbf{R}_B \in \mathbb{R}^{3\times3}$, which relate the world reference frame to the body-fixed reference frames. The velocity of each object's centroid is considered as the overall velocity and is measurable. Denote the velocities in the world coordinate frame as $\mathbf{v}_A \in \mathbb{R}^3$ and $\mathbf{v}_B \in \mathbb{R}^3$. The position and velocity of the obstacle relative to the controlled object are denoted as the relative position $\mathbf{x}_{rel} \in \mathbb{R}^3$ and relative velocity $\mathbf{v}_{rel} \in \mathbb{R}^3$, where

$$\begin{aligned} \mathbf{x}_{\text{rel}} &= \mathbf{r}_B - \mathbf{r}_A, \\ \mathbf{v}_{\text{rel}} &= \mathbf{v}_B - \mathbf{v}_A. \end{aligned} \tag{33}$$

The short-term collision probability is assessed based on the vector relationship between relative position and relative velocity. Assuming no collision at the current time:

- When $\frac{\langle \mathbf{x}_{rel}, \mathbf{v}_{rel} \rangle}{\|\mathbf{x}_{rel}\| \|\mathbf{v}_{rel}\|} \leq 0$, there is a high probability of future collision.
- When $\frac{\langle \mathbf{x}_{rel}, \mathbf{v}_{rel} \rangle}{\|\mathbf{x}_{rel}\| \|\mathbf{v}_{rel}\|} > 0$, collision is unlikely in the future.

Next, the directional projection along the relative velocity vector is utilized to further assess collision conditions. Taking the relative velocity vector as the normal vector, construct a projection plane passing through the origin of the world coordinate frame. Both the controlled object and obstacle are projected onto this plane, resulting in two 2D polygons. For example, a cuboid projects as either a rectangle or hexagon depending on its orientation.

The coordinate transformation for the projection process can be formulated as the following mathematical problem:

Given a point $\mathbf{p} = (p_x, p_y, p_z)^\top$ in the world coordinate frame W and a unit vector $\mathbf{v} = (a, b, c)^\top$, rotate the z-axis (or y-axis) of frame W to align with $\mathbf{v}$ to obtain a new coordinate frame P. The problem requires computing both the rotation matrix ${}^W\mathbf{R}_P$ that transforms coordinates from P to W and the coordinates $\mathbf{p}'$ of point $\mathbf{p}$ expressed in frame P.

- When $c \neq -1$, rotate around the z-axis,

$${}^W\mathbf{R}_P = \begin{pmatrix} \frac{1+c-a^2}{1+c} & -\frac{ab}{1+c} & a \\ -\frac{ab}{1+c} & \frac{1+c-b^2}{1+c} & b \\ -a & -b & c \end{pmatrix}. \tag{34}$$

- When $c = -1$, rotate around the y-axis,

$$ {}^{W}\mathbf{R}_P = \begin{pmatrix} \sqrt{1-a^2} & -\frac{ab}{\sqrt{1-a^2}} & -\frac{ac}{\sqrt{1-a^2}} \\ a & b & c \\ 0 & -\frac{c}{\sqrt{1-a^2}} & \frac{b}{\sqrt{1-a^2}} \end{pmatrix}. \quad (35) $$

And $\mathbf{p}' = {}^{W}\mathbf{R}_P^{\top} \cdot \mathbf{p}$. Recalling the method in Section IV, the vertices of the convex polyhedron are projected onto a 2D plane via ${}^{W}\mathbf{R}_P$, connected counterclockwise to form a convex polygon, padded with the scaling function (23) to ensure strict convexity, and finally the optimization problem (32) is solved to determine the minimal uniform scaling factor α between the two.

This innovative approach avoids projection region intersection, leading to directional projection CBFs, formulated as:

$$ h(x) = \alpha^*(x) - \alpha_0, \ \frac{\langle \mathbf{x}_{rel}, \mathbf{v}_{rel} \rangle}{\|\mathbf{x}_{rel}\| \|\mathbf{v}_{rel}\|} \leq 0, \quad (36) $$

where $\alpha^*(x)$ is the solution to the optimization problem (32), and $\alpha_0 > 0$ is a user-chosen parameter. If the control u is designed such that $h(x) > 0$ holds forward in time, then $\alpha^*(x) > \alpha_0 > 1 + \delta$. This means $S_{s_A} \cap S_{s_B} = \varnothing$ and thus $S_A \cap S_B = \varnothing$. In other words, the collision is avoided.

The set C is defined as the set of safe directions for the relative velocity vector. Given a function $h\colon \mathcal{D} \subseteq \mathbb{R}^n \to \mathbb{R}$ that satisfies the conditions outlined in Definition 1 on C, it follows that a Lipschitz continuous control policy obtained from the corresponding quadratic program (QP) guarantees collision avoidance with the obstacle, even if the reference control signal u_{ref} would otherwise lead to a collision. The physical meaning of the safety set C can be demonstrated through proof by contradiction.

The proposition *"if the projection regions do not intersect, then collision does not occur"* is equivalent to its contrapositive *"if collision occurs, then the projection regions intersect"*. Now suppose there exist non-intersecting projection regions where collision occurs. A collision implies intersection in 3D space, which must result in intersecting projections onto any plane. This contradicts our assumption, thus proving the original proposition.

To ensure that the initial state of the obstacle avoidance process lies within the interior of the safe set $\mathcal{C}$, consider designing α_0 as

$$ \alpha_0 = e^{-\tau \cdot d_{min}} + \delta, \quad (37) $$

where $d_{min} \geq 0$ denotes the minimum distance between the two polyhedrons, and $\tau > 0$ represents a user-chosen parameter. When $a_0 < 1 + \delta$ (which is equivalent to $d_{min} > 0$), it means that no collision occurs. If the polyhedrons is padded to strict convexity using a similar scaling function (23), then the derivative of d_{min} with respect to time t exists. In practice, $\frac{d\alpha_0}{dt}$ can be obtained through numerical differentiation:

$$ \frac{d\alpha_0}{dt} = \frac{\alpha_0(t + \Delta) - \alpha_0(t)}{\Delta}, \quad (38) $$

where Δ is a tiny increment.

The next theorem proves that $\nabla_x h \neq 0$ for $h(x) = 0$.

Theorem 3: For a CBF h defined in (36) with $\alpha_0 = e^{-\tau \cdot d_{min}} + \delta$. If $h(x) = 0$, then $\nabla_x h = \left[\frac{\partial h}{\partial x_1}, \frac{\partial h}{\partial x_2}\right]^{\top} \neq 0$.

Proof: When $h(x) = 0$, we have

$$ \alpha^*(x) = \alpha_0 > \alpha_{desired} + \delta. \quad (39) $$

Thus, $S_A \cap S_B = \varnothing$ (after $\alpha_{desired}$-scaling). If $\nabla_x h = 0$, since $\frac{\partial \alpha_0}{\partial x_2} = 0$, then $\nabla_{x_2} \alpha^* = \nabla_{x_2} h$, no infinitesimally small change in x_2 exists that can change α^*. This is impossible because when $c_A \neq c_B$, there always exists an infinitesimal translation of x_2 that will change the value of α^*. Hence, $\nabla_x h \neq 0$ must be hold. ∎

By Theorem 1, the derivative of h with respect to t yields

$$ \begin{aligned} \frac{dh}{dt} = &\left(\frac{\partial F_A}{\partial z} \cdot \frac{\partial z}{\partial x_2} + \frac{\partial F_A}{\partial x_2} \right) \cdot f_2(x) \\ &+ \left(\frac{\partial F_A}{\partial z} \cdot \frac{\partial z}{\partial x_2} + \frac{\partial F_A}{\partial x_2} \right) \cdot g_2(x) u \\ &+ \left(\frac{\partial F_A}{\partial z} \cdot \frac{\partial z}{\partial x_1} + \frac{\partial F_A}{\partial x_1} \right) \cdot x_2 - \dot{\alpha}_0, \end{aligned} \quad (40) $$

where $\frac{\partial z}{\partial x_1}$ and $\frac{\partial z}{\partial x_2}$ are given by the equation (12). Then the set of admissible controls is following:

$$ K_{cbf}(x) = \left\{ u \in \mathcal{U} \,\middle|\, \frac{dh}{dt} \geq -\Gamma(h(x)) \right\}. \quad (41) $$

VI. SIMULATION STUDIES

This section demonstrates the effectiveness of the proposed method. First, the performance of the approach is illustrated through a simulated mobile robot scenario. Subsequently, the method is applied to a 7-DOF robotic arm, and its performance is validated in simulation.

A. Simulation 1: Obstacle Avoidance of Mobile Robot

Consider the unicycle model for a wheeled mobile robot given by $\dot{x} = v\cos\theta$, $\dot{y} = v\sin\theta$, $\dot{v} = u_2$, $\dot{\theta} = u_1$, where x, y denote the location, θ is the heading angle, v denotes the linear speed, and u_1, u_2 are the two control inputs (turning speed and forward acceleration).

The initial setup is illustrated in Fig. 3 (a), where the red rectangle ($3m \times 2m$) represents the mobile robot, and the blue rectangle ($3m \times 2m$) and green rectangle ($3m \times 2m$) represents the obstacles. Assuming the velocity direction is parallel to the longer side of the rectangle, the tracking trajectory for the mobile robot is a straight line with a heading angle of 45 degree. The robotic initial velocity is $(0, 0)^{\top}$ m/s, while the obstacles move with constant velocity $(0.5, -0.2)^{\top} m/s$ and along a circular arc (initial velocity $(-0.1, -0.2)^{\top} m/s$, angular velocity $-0.07\ rad/s$), respectively.

This problem occurs in 2D space, where the projection process along the relative velocity direction simplifies to the projection of polygons onto line segments. The computation of scaling factors for two line segments is straightforward and does not require solving an optimization problem :

$$ \alpha = \frac{2d}{L_1 + L_2}, \quad (42) $$

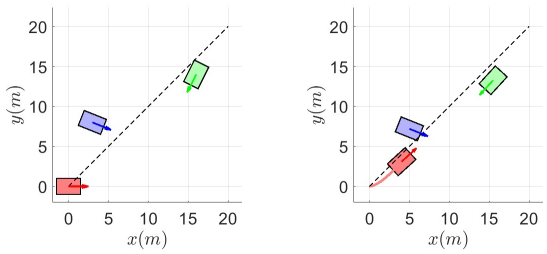

(a) t = 0 s (b) t = 4 s

(c) t = 8 s (d) t = 14 s

Fig. 3: Obstacle avoidance of mobile robot. The black dashed line denotes the tracking trajectory, and the red solid line the actual trajectory. (a) Initial positions of the mobile robot and obstacles. (b)-(d) Relative positions between the mobile robot and obstacles at different time instants.

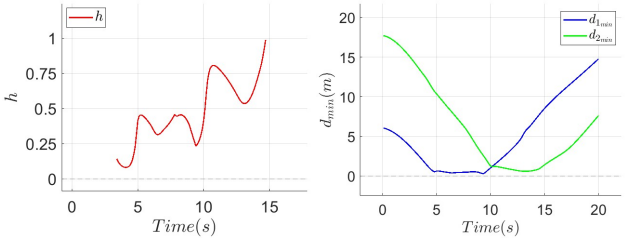

(a) Values of h (b) Minimum distance

Fig. 4: Obstacle avoidance of mobile robot. (a) Values of the CBF h. (b) Minimum distance between the mobile robot and obstacles. $d_{1_{min}}$ is the minimum distance between the mobile robot and the blue obstacle, and $d_{2_{min}}$ is the minimum distance to the red obstacle.

where d is the distance between the centers of the two line segments, and L_1 and L_2 are the lengths of the two line segments, respectively. The perception range of the mobile robot was simulated as the triggering condition for the CBF constraint, satisfying: $\frac{\langle \mathbf{x}_{\text{rel}}, \mathbf{v}_{\text{rel}} \rangle}{\|\mathbf{x}_{\text{rel}}\| \|\mathbf{v}_{\text{rel}}\|} \leq 0$.

Fig. 3 (b)–(d) show the relative positions between the mobile robot and obstacles at different time instants, demonstrating the entire obstacle avoidance process. It is evident that the mobile robot initiated an obstacle avoidance maneuver some time before the collision occurred. The values of the CBF h defined in (36) are presented in Fig. 4 (a). As expected, $h \geq 0$ holds throughout the simulation, ensuring collision avoidance. Considering the non-intuitive physical interpretation of the defined CBF, the minimum distance between the mobile robot and obstacles was computed as a reference (Fig. 4 (b)), where $d_{\text{min}} \geq 0$ is maintained.

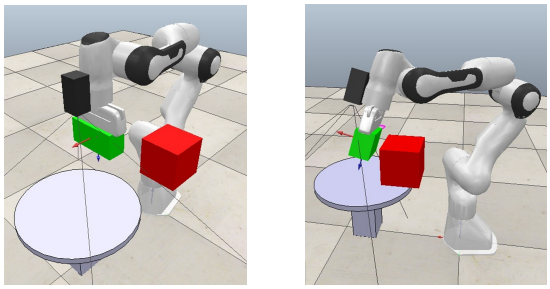

(a) t = 0 s (b) t = 1.2 s

(c) t = 3 s (d) Tracking trajectory

Fig. 5: Obstacle avoidance of Franka arm's end-effector. (a) Initial positions of the Franka arm and obstacle. (b) Relative positions between the Franka arm and obstacle at time $t = 1.2s$. (c) Actual trajectory. (e) Tracking trajectory.

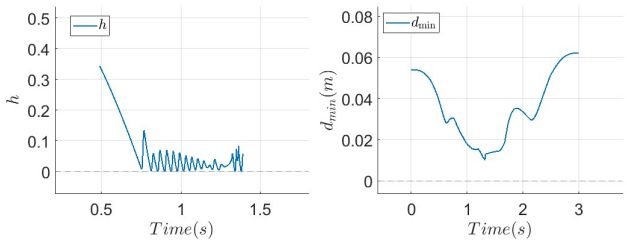

(a) Values of h (b) Minimum distance

Fig. 6: Obstacle avoidance of Franka arm's end-effector. (a) Values of the CBF h. (b) Minimum distance between the Franka arm's end-effector and obstacle.

B. *Simulation 2: Obstacle Avoidance of Franka Arm's End-effector*

To verify the efficacy of the proposed method, a simulation is conducted on a virtual Franka Emika manipulator with 7 DOF in the open-source robot simulation software Coppeliasim.

Consider the scenario shown in Fig. 5, where the target is the green cuboid block($0.16m \times 0.08m \times 0.06m$) grasped by the robotic arm's end-effector and the obstacle is the red cubic block($0.12m \times 0.12m \times 0.12m$). The experimental task involves controlling the robotic arm to make the green block follow a specified trajectory while avoiding the obstacle. The

nominal controller for the robotic arm is backstepping control

$$\begin{aligned}\tau = M(q)\cdot[-(1+k_1k_2)\,e_q-(k_1+k_2)\,e_{\dot{q}} \\ +\ddot{q}_d]+C(q,\dot{q})+G(q),\end{aligned} \tag{43}$$

where $k_1, k_2 > 0$ are tunable control parameters. The joint torques are then transformed into end-effector wrenches by $\mathcal{F} = (J_b^\dagger)^\top \tau$, and our CBF constraints are applied in Cartesian space:

$$\mathcal{F} = M_{\mathbf{x}}(q)\ddot{\mathbf{x}} + C_{\mathbf{x}}(q,\dot{q}) + G_{\mathbf{x}}(q), \tag{44}$$

where $M_{\mathbf{x}}(q) \in \mathbb{R}^{n\times n}$ represents the Cartesian mass matrix, $C_{\mathbf{x}}(q,\dot{q}) \in \mathbb{R}^n$ represents the Coriolis and centrifugal vector in Cartesian space, and $G(q) \in \mathbb{R}^n$ represents the gravity vector in Cartesian space. Finally, redundant degrees of freedom are scheduled through null-space projection

$$\tau^* = J^\top \cdot \mathcal{F}^* + \left(\mathbf{I} - J^\dagger J\right)\cdot \tau. \tag{45}$$

where $\mathcal{F}^*$ is the CBF-QP-compensated force. Additionally, if point $\mathbf{p}$ is a vertex of the polygon A, we have:

$$\begin{aligned} {}^B\mathbf{p} &= {}^BR_E \cdot {}^E\mathbf{p} + {}^{\mathbf{B}}\mathbf{p}_{\mathbf{E}}, \\ \frac{d^B\mathbf{p}}{d\mathbf{x}} &= [I \quad -[{}^BR_E \cdot {}^B\mathbf{p}]_\times], \end{aligned} \tag{46}$$

where B represents the base coordinate frame, E represents the end-effector coordinate frame, and $[\cdot]_\times$ is the skew-symmetric matrix of a vector.

The initial joint angles of the robotic arm are $q_0 = (0,\, -45^\circ,\, 0,\, -135^\circ,\, 0,\, 90^\circ,\, 45^\circ)^{\mathrm{T}}$, and the initial position of the obstacle center is $p_{\text{obs}} = (0.2,\, 0.19,\, 0.48)^{\mathrm{T}}$ (see Fig. 5 (a)). Fig. 5 (b) shows the relative positions between the target and obstacle at time $1.2s$ during collision avoidance, where no collision occurs. Fig. 5 (c) displays the complete trajectory of the target center from a top view perspective, while Fig. 5 (d) shows the tracking trajectory (a circular arc with radius $r = 0.3\,\text{m}$) without CBF constraints, which intersects the obstacle region. The values of h are shown in Fig. 6 (a) and the minimum distance are shown in Fig. 6 (b). As shown in Fig. 6, both $h \geq 0$ and $d_{\min} \geq 0$ hold throughout the simulation, ensuring collision avoidance and verifying a safe operational margin, respectively.

VII. CONCLUSIONS

For second-order robotic systems, a directional projection CBFs design method based on differentiable optimization is proposed to avoid collisions with various shapes of static and dynamic obstacles, particularly polyhedra. Inspired by the human eye's obstacle avoidance mechanism, potential collisions are proactively detected by projecting perspectives along the relative velocity direction. Specifically, tunable uniform scaling functions are employed to pad convex polygons with versions of various sizes, achieving higher accuracy compared to using one or multiple circles for padding. The method has been successfully validated on a 2D mobile robot and a 7-DOF Franka manipulator. Future work will consider interference factors in practical applications, particularly relative velocity perturbations, as well as improving real-time computational efficiency.

REFERENCES

[1] Z. Yang, "Research and application of industrial robot control system," in *2024 Asia-Pacific Conference on Software Engineering, Social Network Analysis and Intelligent Computing (SSAIC)*, 2024, pp. 910–912.

[2] N. El Yasmine Aichaoui, "Enhancing safety protocols for human-robot collaboration in welding environments: Investigation review into augmenting worker safety within robot hazard zones," in *2024 IEEE 22nd World Symposium on Applied Machine Intelligence and Informatics (SAMI)*, 2024, pp. 000 035–000 040.

[3] J. G. Leem, D. J. Kim, M. H. Lee, S. J. Kim, and J. H. Suh, "Robust tracking model predictive control scheme for application to differential mobile robot for trajectory tracking," in *2024 24th International Conference on Control, Automation and Systems (ICCAS)*, 2024, pp. 947–949.

[4] Q. Liu, C.-Y. Chen, C. Wang, and W. Wang, "Common workspace analysis for a dual-arm robot based on reachability," in *2017 IEEE International Conference on Cybernetics and Intelligent Systems (CIS) and IEEE Conference on Robotics, Automation and Mechatronics (RAM)*, 2017, pp. 797–802.

[5] N. Zhang, Y. Zhang, C. Ma, and B. Wang, "Path planning of six-dof serial robots based on improved artificial potential field method," in *2017 IEEE International Conference on Robotics and Biomimetics (ROBIO)*, 2017, pp. 617–621.

[6] A. D. Ames, S. Coogan, M. Egerstedt, G. Notomista, K. Sreenath, and P. Tabuada, "Control barrier functions: Theory and applications," in *2019 18th European Control Conference (ECC)*, 2019, pp. 3420–3431.

[7] K. Tracy, T. A. Howell, and Z. Manchester, "Differentiable collision detection for a set of convex primitives," in *2023 IEEE International Conference on Robotics and Automation (ICRA)*, 2023, pp. 3663–3670.

[8] B. Dai, R. Khorrambakht, P. Krishnamurthy, V. Gonçalves, A. Tzes, and F. Khorrami, "Safe navigation and obstacle avoidance using differentiable optimization based control barrier functions," *IEEE Robotics and Automation Letters*, vol. 8, no. 9, pp. 5376–5383, 2023.

[9] S. Wei, B. Dai, R. Khorrambakht, P. Krishnamurthy, and F. Khorrami, "Diffocclusion: Differentiable optimization based control barrier functions for occlusion-free visual servoing," *IEEE Robotics and Automation Letters*, vol. 9, no. 4, pp. 3235–3242, 2024.

[10] W. Xiao and C. Belta, "High-order control barrier functions," *IEEE Transactions on Automatic Control*, vol. 67, no. 7, pp. 3655–3662, 2022.

[11] Y. Wei, Y. Feng, L. Ou, Y. Wang, and X. Yu, "Explicit solution of tunable input-to-state safe-based controller under high-relative-degree constraints," *IEEE Transactions on Automatic Control*, pp. 1–8, 2025.

[12] S. Wei, R. Khorrambakht, P. Krishnamurthy, V. Mariano Gonçalves, and F. Khorrami, "Collision avoidance for convex primitives via differentiable optimization-based high-order control barrier functions," *IEEE Transactions on Control Systems Technology*, pp. 1–16, 2025.

[13] A. Chakravarthy and D. Ghose, "Obstacle avoidance in a dynamic environment: a collision cone approach," *IEEE Transactions on Systems, Man, and Cybernetics - Part A: Systems and Humans*, vol. 28, no. 5, pp. 562–574, 1998.

[14] P. Thontepu, B. G. Goswami, M. Tayal, N. Singh, S. S. P I, S. S. M G, S. Sundaram, V. Katewa, and S. Kolathaya, "Collision cone control barrier functions for kinematic obstacle avoidance in ugvs," in *2023 Ninth Indian Control Conference (ICC)*, 2023, pp. 293–298.

[15] B. G. Goswami, M. Tayal, K. Rajgopal, P. Jagtap, and S. Kolathaya, "Collision cone control barrier functions: Experimental validation on ugvs for kinematic obstacle avoidance," in *2024 American Control Conference (ACC)*, 2024, pp. 325–331.

[16] M. Tayal, R. Singh, J. Keshavan, and S. Kolathaya, "Control barrier functions in dynamic uavs for kinematic obstacle avoidance: A collision cone approach," in *2024 American Control Conference (ACC)*, 2024, pp. 3722–3727.

[17] H. K. Khalil, *Nonlinear Systems*, 3rd ed. Upper Saddle River, N.J.: Prentice Hall, 2002.

[18] F. Nielsen and K. Sun, "Guaranteed bounds on the Kullback-Leibler divergence of univariate mixtures using piecewise log-sum-exp inequalities," *IEEE Signal Processing Letters*, vol. 23, no. 11, pp. 1541–1545, Nov. 2016.

[19] A.-L. Cauchy, *Cours d'Analyse de l'École Royale Polytechnique*. Paris, France: l'École Royale Polytechnique, 1821.